Formation of Vertical Concentration Gradients in Poly(3-hexylthiophene-2,5-diyl) : Phenyl-C_{61}-butyric acid methyl ester Graded Bilayer Solar Cells

Varun Vohra[a,*], Koichi Higashimine[b], Shogo Tsuzaki[a], Keisuke Ohdaira[c], and Hideyuki Murata[a,*]

[a] *School of Materials Science, Japan Advanced Institute of Science and Technology, 1-1 Asahidai, Nomi, Ishikawa 923-1292, Japan*

[b] *Nano-material Technology Center, Japan Advanced Institute of Science and Technology, 1-1 Asahidai, Nomi, Ishikawa 923-1292, Japan*

[c] *Green Devices Research Center, Japan Advanced Institute of Science and Technology, 1-1 Asahidai, Nomi, Ishikawa 923-1292, Japan*

Abstract

In the present work, we demonstrate that graded bilayer solar cells provide a very interesting alternative to the bulk heterojunction active layers commonly used in organic photovoltaic cells. One of the main advantages of this type of active layers is the possibility to optimize independently both donor and acceptor layers. Using various process methods, we obtain active layers that demonstrate a donor-acceptor vertical concentration gradient. These devices exhibit not only a high fill factor but also a remarkable increase in open-circuit voltage (V_{oc}). In order to understand the influence of the film morphology over the device parameters, we provide a complete study using energy-dispersive X-Ray spectroscopy elemental mapping of the device cross-sections which shows evidence that ideal donor-acceptor concentration gradient are required to obtain high fill factors. Furthermore, we use a simple equivalent electrical model to extrapolate device parameters such as reverse saturation current for a clearer understanding of the origin of the V_{oc} increase.

Keywords: Organic solar cells, nanostructures, self-assembly, P3HT

* Corresponding author. Tel.: +81 761 51 1531; fax: +81 761 51 1149 (H. Murata)

E-mail addresses: murata-h@jaist.ac.jp (H. Murata), varunvohra1984@gmail.com (V. Vohra)

1. Introduction

Bulk heterojunction (BHJ) organic solar cells have been widely studied over the past decade as they provide an easy method to obtain high performance solar cells [1, 2]. However, as both donor and acceptor materials are processed simultaneously; it becomes difficult to enhance their independent properties in order to further improve the performances. Researchers studying the most commonly used Poly(3-hexylthiophene-2,5-diyl) (P3HT):Phenyl-C_{61}-butyric acid methyl ester (PCBM) donor:acceptor system have recently introduced a method to consequently deposit the donor and acceptor layers by solution process [3,4]. The key to this process resides in using a solvent in which PCBM is soluble and which swells P3HT without dissolving it to form active layers referred to as graded bilayers (GB). More specifically, dichloromethane (DCM) can dissolve PCBM and only swells the amorphous parts of P3HT [5].

This alternative approach demonstrated equivalent or higher results than the commonly used BHJ active layers [6]. More specifically, recent results in both our and other laboratories demonstrated power conversion efficiencies (PCE) up to 4% [7-9], as compared to an average PCE of 2.8% for BHJ prepared in our laboratory. Our study focuses on various methods to control the crystallinity of P3HT and study its influence

on the device performances and vertical concentration formation. These methods consist in nanostructuration of P3HT by self-assembly with polystyrene (PS) [10] and addition of regiorandom P3HT (RRa-P3HT) to the regioregular P3HT (RR-P3HT) [9] used for device fabrication. We compare the results obtained using these various fabrication methods and through a morphological study of the active layer, we will confirm that crystallinity plays a key role in the formation of ideal vertical concentration gradients as DCM mainly swells the amorphous parts of P3HT. After a careful analysis of the device performances in correlation with a study of the cross-sections using energy-dispersive x-ray spectroscopy (EDS) elemental mapping, we define the ideal vertical concentration gradient in GB solar cells.

2. Experimental Details

RR-P3HT (Mw = 21 000 $g.mol^{-1}$) and PCBM were purchased from Merck and Luminescence Technology, respectively, while RRa-P3HT and PS (Mw = 45 000 $g.mol^{-1}$) were acquired from Sigma Aldrich. Glass substrates coated with 150 nm thick indium tin oxide layers are used as the anode. After a standard cleaning procedure and exposure to UV irradiation, they are covered with 35 nm of poly(3,4-ethylenedioxythiophene) poly(styrenesulfonate) (Clevios P, H. C. Starck, 4000

rpm for 60s, annealed at 200˚C for 10 min). P3HT and P3HT:PS solutions were prepared at a concentration of 30 mg.ml^{-1} in chlorobenzene and spin-coated at either 1500 (for the study on self assembled nanostructures with PS) or 2500 rpm for 30s on top of poly(3,4-ethylenedioxythiophene) poly(styrenesulfonate). In the case of blends with PS, the films were consequently dipped in acetone to remove PS prior to PCBM deposition. PCBM solution (10mg.ml^{-1}) was deposited at either 2000 rpm for 30s (for the nanostructured P3HT study) or 4000 rpm for 10s (in the case of additional RRa-P3HT). The variations in the reference device performances originate from the necessity to have thicker P3HT films for nanostructuration. The PCBM spin-coating conditions were consequently optimized for the thicker P3HT layers.

Film thicknesses were measured by scratching the film and measuring the height difference across the scratch using an AFM from Keyence (Nanoscale Hybrid Microscope VN-8000). The active layer thickness of nanostructured and additional RRa-P3HT devices are typically 130 and 125 nm, respectively. Absorption spectra were measured using a Jasco V670 UV/Vis Spectrometer.

All devices were finalized by evaporating a 100 nm thick Aluminum cathode under vacuum (10^{-4} Pa) and encapsulated with a glass cap using an ultraviolet curing epoxy resin inside a nitrogen filled glovebox. The devices were further post annealed at

140°C for 10 min. The active areas were shadowed during the 15-min exposure to the UV radiation to avoid photodegradation of the organic layers. The device active area is 2 mm^2.

The current–voltage characteristics of the encapsulated devices were measured in air, using a Keithley 2400 Sourcemeter and a Solar simulator at one sun light irradiance (AM 1.5, 100mW/cm^2) at room temperature. Photoelectron Yield Spectra were measured using a AC-2 Spectrometer from Riken Keiki.

EDS for elemental analysis was carried out with a scanning transmission electron microscope, JEM-ARM200F from JEOL. The acceleration voltage and probe current were 200 kV and 59 pA, respectively to obtain 256 x 256 pixels images with a dwell time of 1 ms/pixel. Each image was accumulated for 120 s to improve the signal to noise ratio.

3. Results and discussion

P3HT thin films are usually composed of a crystalline and an amorphous part. Previous studies have demonstrated that the deposition of the PCBM layer does not disturb the order in the P3HT layer as DCM only swells the amorphous P3HT [5]. Using self-assembly between two polymers, namely, P3HT and PS, we were able to fabricate nanostructured thin films of P3HT. With the help of Fourier transform infrared

spectroscopy (FTIR) and ellipsometry, we previously demonstrated that the resulting P3HT films consist of a wetting layer and a nanoporous top layer [10]. The two parts of the P3HT films have different crystallinities. More specifically, both FTIR and ellipsometry confirmed that the nanoporous part is more amorphous than the wetting layer (and also more amorphous than the P3HT films with no nanostructure). With this difference in crystallinity in mind, we intended to study the diffusion of PCBM inside the P3HT films in the vertical and horizontal directions inside the pores. After PCBM deposition, the films were soaked in cyclohexanone (a good solvent for PCBM but non solvent for P3HT) to dissolve the PCBM rich regions of the films.

The AFM images, prior to PCBM deposition and after soaking in cyclohexanone, show a clear widening and deepening of the pores (Fig. 1). When considering a single pore, we observe that the widening of its diameter corresponds to around 75nm on each side while the deepening (taking into account the reduction of the total film thickness) is only about 60 nm. This result confirms that different diffusion behaviors can be observed in the crystalline wetting layer and more amorphous nanostructured parts of the film.

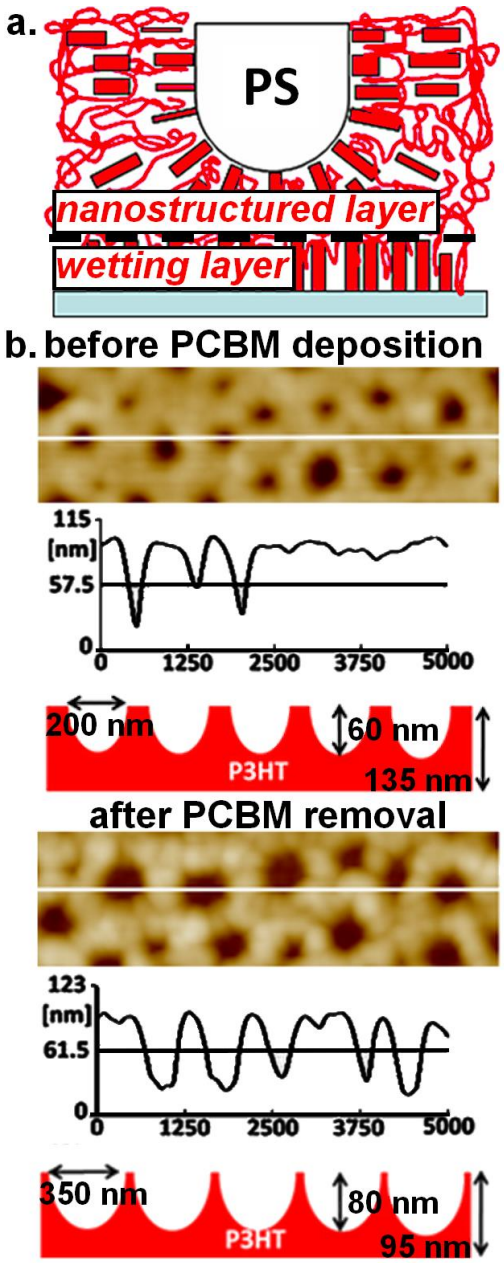

Fig. 1: (a) schematic representation of the P3HT chains in nanostructured thin P3HT films and (b) morphological changes of the P3HT porous structure before and after PCBM deposition

The influence on the device performances (Table I) upon nanostructuration is quite remarkable with an increase in PCE of about 30 % mainly resulting from a fill

factor (*FF*) increase from around 40 % to 50 %. The significant reduction in series resistance (R_s) also induces a slight increase in open-circuit voltage (V_{oc}). The apparent short-circuit current ($J_{sc)}$ remains almost unchanged. However, the films with 25 wt% of PS have an aborption intensity that corresponds to 74.5% of the absorption of the pure P3HT films. The unchanged J_{sc} is therefore the result of two opposite effects: on the one hand, the decrease in amount of P3HT results in less light absorption and consequently, less exciton generation, while on the other hand, the better mixing with the introduced nanostructured amorphous part and the consequent formation of a vertical concentration gradient induces better charge separation and transport to the respective electrodes.

Table I: Summary of photovoltaic performances of regular (0 PS wt%) and nanostructured bilayers (20 PS wt%)

PS wt%	J_{sc} **(mA/cm^2)**	V_{oc} **(V)**	***FF*** **(%)**	**PCE (%)**
0	10.8	0.57	41	2.51
25	10.5	0.61	51	3.25

This confirms that crystallinity plays a key role in the fabrication of ideal vertical concentration gradient devices. The ideal structure for the bottom P3HT layer consists of a crystalline lower part and an amorphous top part which would respectively serve as a crystalline buffer layer with efficient hole transport properties and an

interfacial layer allowing for good mixing with PCBM for efficient charge generation. By adding RRa-P3HT to RR-P3HT, such device architectures can be obtained and the vertical concentration gradient as well as the thickness of the P3HT buffer layer can be tuned.

Using EDS elemental mapping, we obtain accurate information about the vertical composition along the cross-section of the devices (Fig. 2). The devices were post annealed at 140˚C for 10 min after Aluminum deposition. This process is well-known for BHJ as it enhances the device performances through an increase of V_{oc} and *FF* related to changes in the active layer morphology [11]. Such thermal treatment induces surface tension and phase separation driven diffusion and reorganization of the molecules in the active layers [12]. In Fig. 2, we can observe that in the case of RR-P3HT active layers, P3HT diffuses at both interfaces trapping the PCBM between two P3HT rich (electron blocking) layers. By adding small amounts of RRa-P3HT (5wt%), the diffusion of P3HT towards the top electrode is limited. Upon addition of 10 wt% and more, no more P3HT can be found in contact with the aluminum electrodes. Through the addition of RRa-P3HT, we can control the diffusion of P3HT to the top electrode thus obtaining various concentration gradient profiles.

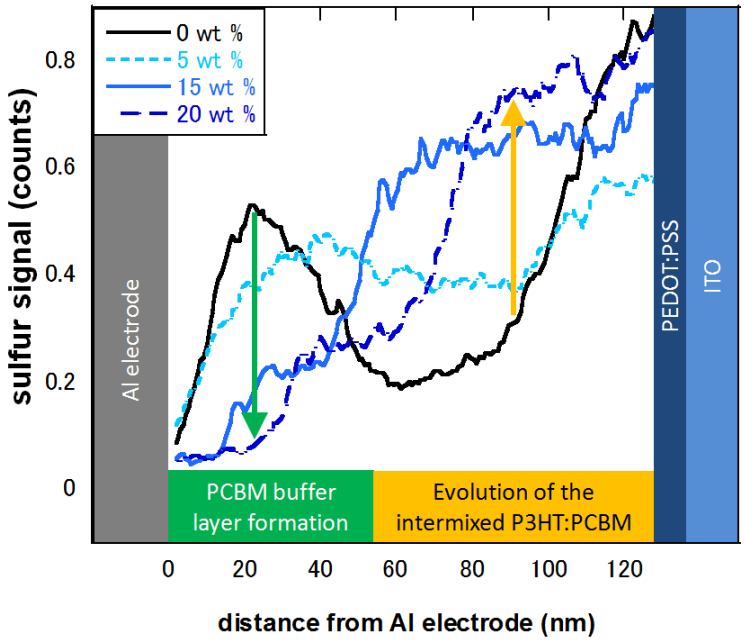

Fig. 2: Evolution of the sulfur concentration profile with increasing RRa-P3HT concentration. The green and yellow arrows respectively represent the decrease of P3HT close to the Al electrode and the changes in P3HT concentration through the intermixed layer.

The diffusion of P3HT molecules towards both electrodes upon annealing has been observed similarly in the case of BHJ solar cells in our laboratory. Previous studies have demonstrated the influence of the surface tension of each of the materials at an interface by comparing annealing under the same conditions with and without the top aluminum electrode [4]. The data that we collected demonstrates that the addition of amorphous material to the active layer gradually decreases such vertical P3HT

movements.

Thermal treatment allows for molecules to reorganize which leads to a larger phase separation in the case of systems such as RR-P3HT:PCBM BHJ. More specifically, with the energy provided to the system during annealing, the amorphous regions of RR-P3HT will rearrange resulting in the formation of large P3HT and PCBM domains (as observed in the case of the 0 wt% films). The introduction of RRa-P3HT which cannot crystallize and mixes well with PCBM therefore reduces the strength of that repulsion between P3HT and PCBM which we believe is at the origin of the different concentration profiles obtained with various amounts of RRa-P3HT.

Table II displays the device performances obtained with various amounts of RRa-P3HT. The addition of RRa-P3HT results in a blue shift of the P3HT absorption as well as a decrease in absorption intensity. Consequently, an irregular trend can be observed for J_{sc} as less absorption results in less charge generation.

Table II: Evolution of device performances with various RRa-P3HT contents

RRa-P3HT (wt%)	J_{sc} **(mA/cm^2)**	V_{oc} **(mV)**	***FF*** **(%)**	**PCE (%)**
0	10.05	594	51.8	3.09
5	9.49	599	54.0	3.08
15	10.34	617	60.1	3.83
20	9.40	621	59.6	3.48

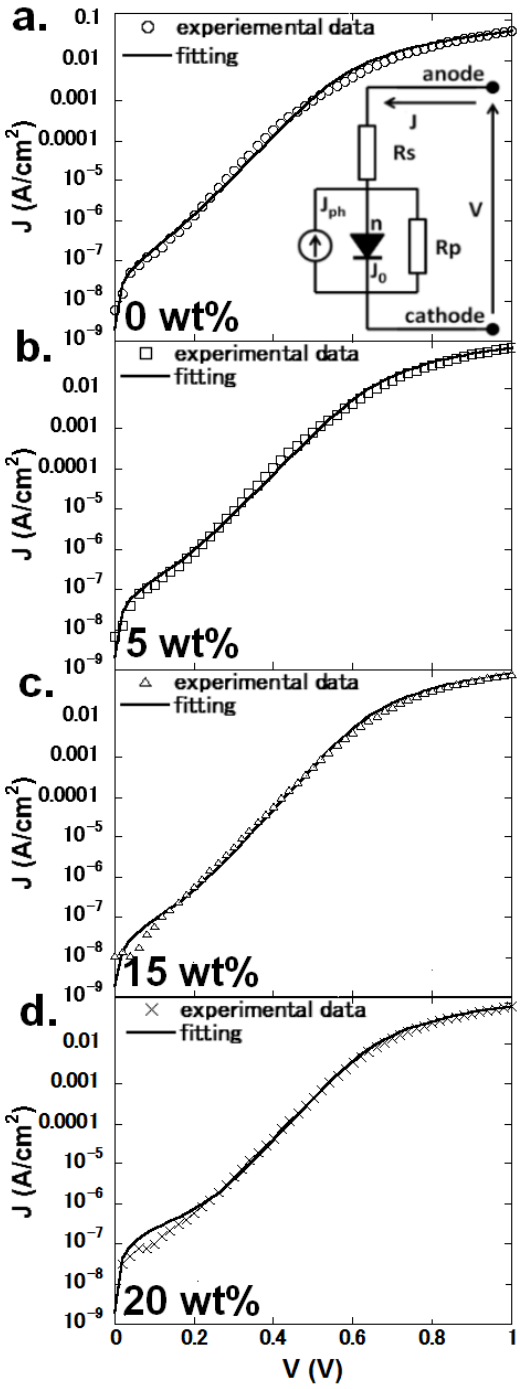

Fig. 3: experimental *J-V* curves and fittings of devices with (a) 0, (b) 5, (c) 15 and (d) 20 wt% of RRa-P3HT and (inset of (a)) equivalent circuit model for the dark J-V curve fitting

The changes observed in V_{oc} are partially related to changes in the highest

occupied molecular orbital (HOMO) level between crystalline and amorphous P3HT as well as the changes in Rs [13]. Previous studies in literature have demonstrated that V_{oc} is not only related to the electronic properties of the donor and acceptor materials (difference between the HOMO of the donor and the lowest unoccupied molecular orbital of the acceptor) but also to the parameters of the equivalent electrical circuit (Fig. 3a) [11]. More specifically, the inverse saturation current (J_0) and the ideality factor (n) account for the leaks in the devices (e.g. holes collected at the Al electrode) and for the charge recombination inside the thin active layers, respectively.

An ideal device would have a very low J_0 (no leak) and an ideality factor of 1 (no recombination). These parameters can be obtained by fitting the dark *J-V* characteristics using the equivalent circuit equation:

$$J = Jo\left\{\exp\left[\frac{e(V - JARs)}{nk_BT}\right] - 1\right\} + \frac{(V - JARs)}{R_pA} - J_{ph}$$

where *Rp* is the parallel resistance, *e* the elementary charge, k_B the Boltzmann constant, T the temperature, J_{ph} the photogenerated current density and A the device area. The results are displayed in Table III.

Table III: Device parameters obtained using the fittings of the dark J-V

RRa-P3HT (wt%)	***J_0*** **(10^{-9}A.cm^{-2})**	***n***	***Rs*** **(Ω.cm^2)**	***Rp*** **(MΩ.cm^2)**
0	11.9	1.67	6.43	1.05
5	7.73	1.70	2.71	0.89
15	2.61	1.58	2.33	1.64
20	2.45	1.61	3.24	0.46

To understand the effect of J_0 and n on the V_{oc}, the equivalent circuit equation can be simplified when $J = 0$ ($V = V_{oc}$). The equivalent circuit equation is reduced (details in [11]) to the following where V_{oc} can be related to n and J_0:

$$Voc \approx \frac{nk_BT}{e} \ln\left[\frac{Jsc}{Jo}\right]$$

The increase in V_{oc} that we observe is therefore not only related to the changes in HOMO of the P3HT layer but also to the decrease in J_0 which results from the changes in vertical concentration gradient. The GB devices with no RRa-P3HT have a large amount of P3HT at the aluminum electrode interface which results in leak current. This electron blocking layer is gradually removed leading to a decrease of J_0 of almost one order of magnitude (20 RRa wt% devices).

The influence of the ideality factor on the V_{oc} is minor compared to that of J_0. However, it provides useful information on the charge recombination within the film.

The ideal case (no recombination, n=1) can rarely be observed in organic solar cells. With the values obtained from the fitting, we can observe a slight increase of n when adding 5 wt% of RRa-P3HT. From Fig. 2, the active layer containing 5 wt% of RRa-P3HT displays an almost homogenous concentration of P3HT throughout the film. Even though less P3HT can be found close to the aluminum electrode, this lack of vertical concentration gradient leads to a high probability of recombination (both P3HT and PCBM can be found all along the vertical direction in the active layer). On the other hand, the introduction of a PCBM buffer layer and a concentration graded structure (15-20 RRa-P3HT wt%) reduces the ideality factor value.

To further understand the effect of the vertical concentration gradient, we will now focus on *FF* and Rs and relate the morphologies observed with EDS to these characteristics. We should keep in mind that Rs is also related to the intrinsic charge transport properties of the materials and that the hole transport in P3HT is closely related to its crystallinity (higher crystallinity results in better hole transport).

Fig. 4 displays a schematic representation of the film morphology and how it influences the *FF* and *Rs* of the devices. In fact, we can observe that, as the electron blocking P3HT-rich layer in contact with the top electrode disappears upon addition of 5 wt% of RRa-P3HT, the *Rs* of the device decreases due to a better electron collection.

An increase in *FF* from 52 to 54 % can be observed. By further increasing the RRa-P3HT content to 15 wt%, a PCBM buffer layer (around 15 nm) is formed. Furthermore, a concentration gradient is formed within the P3HT bottom layer which results in efficient charge generation and hole collection (P3HT rich layer close to the PEDOT:PSS). These two morphological aspects considerably reduce the *Rs* leading to a *FF* reaching 60%.

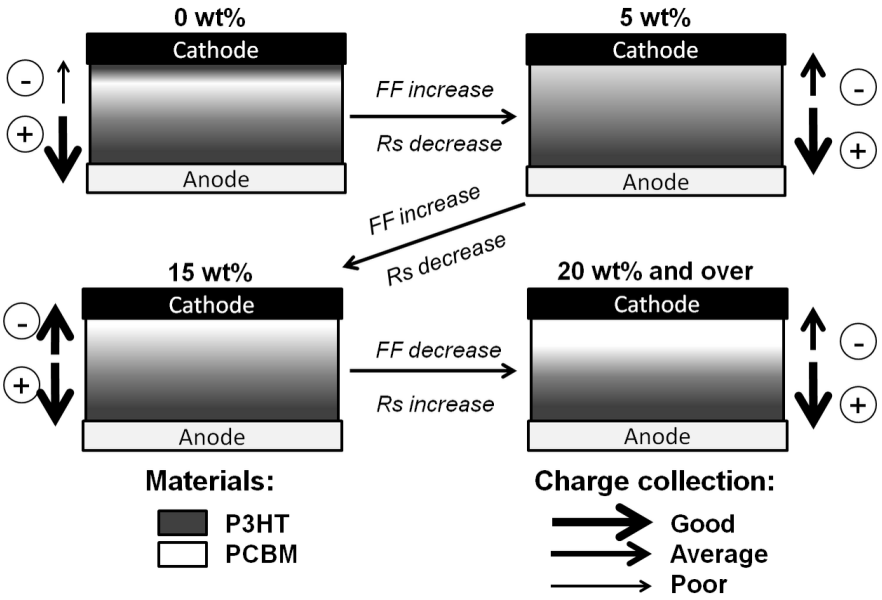

Fig. 4: schematic representation of the evolution of vertical concentration related to device parameters and charge collection efficiency

The increase in *Rs* (decrease in *FF*) observed when the RRa-P3HT contents exceed 15 wt% can be associated with two phenomena. The former is related to the intrinsic hole transport properties of RRa-P3HT. By adding RRa-P3HT to the RR-P3HT

film, the holes are transported less efficiently which results in an increase in *Rs*. The second phenomenon is a direct consequence of the concentration profile observed in the active layer. The PCBM buffer layer gets thicker and the electrons generated at the donor-acceptor interfaces therefore need to travel on a larger distance to be collected at the aluminum electrode.

Taking into account the EDS data and concentration profile/device performances correlation presented previously, we can assume that the ideal GB device is obtained with a concentration graded 80 nm thick layer sandwiched between thin (15 to 20 nm) P3HT and PCBM buffer layers. Furthermore, if such devices can be obtained without the use of RRa-P3HT (lower intrinsic properties), the device performances may exceed the ones presented in this work both in terms of J_{sc} and *FF*.

4. Summary

We demonstrated that using GB instead of BHJ offers the advantage of independently optimizing the P3HT bottom layer prior to PCBM deposition to enhance device performances. Our nanostructured devices exhibit an increase in PCE of 30% compared to the reference cells.

One of the key parameters in organic photovoltaics is the vertical concentration

gradient created within the donor-acceptor active layers. By fitting the dark *J-V* to the equation of a simple electrical circuit, we demonstrated that the origin of the V_{oc} increase in our devices is not only related to a deeper HOMO level of RRa-P3HT but also the result of a decrease of J_0 (related to a better vertical concentration gradient in the active layers). The study presented here further demonstrates that a good correlation between the quality of the concentration gradient and the *FF* of the devices. Through the addition of RRa-P3HT, we can control the diffusion of P3HT to the top electrode and get closer to the ideal vertical concentration gradient. The *FF* obtained for the best devices reach 60%.

EDS sulfur profiles of the cross sections of the devices show a nice evolution and we can predict the ideal structure for a P3HT:PCBM active layer: an intermixed layer of P3HT:PCBM of about 80 nm displaying a concentration gradient and sandwiched between two buffer layers of around 15 to 20 nm. This study confirms that EDS can be a powerful tool to study the active layer of the devices in a non destructive manner and that active layer morphology is as important as the intrinsic properties of the materials used to fabricate photovoltaic cells.

Acknowledgements

The work was supported by a Grant-in-Aid for Scientific Research on Innovative Areas (No. 20108012, "pi-Space") from the Ministry of Education, Culture, Sports, Science, and Technology, Japan. V. Vohra would like to greatly acknowledge financial support through research fellowships from the Japan Society for Promotion of Science for postdoctoral fellowships for foreign researchers.

References

[1] J. Peet, A. J. Heeger, G. C. Bazan, Acc. Chem. Res. 42 (2009) 1700.

[2] G. Dennler, M. C. Scharber, C. J. Brabec, Adv. Mater. 21 (2009) 1323.

[3] A. L. Ayzner, C. J. Tassone, S. H. Tolbert, B. J. Schwartz, J. Phys. Chem. C 113 (2009) 20050.

[4] K. H. Lee, P. E. Schwenn, A. R. G. Smith, H. Cavaye, P. E. Shaw, M. James, K. B. Krueger, I. R. Gentle, P. Meredith, P. Burn, Adv. Mater. 23 (2011) 766.

[5] A. L. Ayzner, S. C. Doan, B. Tremolet de Villers, B. J. Schwartz, J. Phys. Chem. Lett. 3 (2012) 2281.

[6] C. W. Rochester, S. A. Mauger, A. J. Moulé, J. Phys. Chem. C 116 (2012) 7287.

[7] A. Loiudice, A. Rizzo, M. Biasiucci, G. Gigli, J. Phys. Chem. Lett. 3 (2012) 1908.

[8] V. Vohra, G. Arrighetti, L. Barba, K. Higashimine, W. Porzio, H. Murata, J. Phys. Chem. Lett. 3 (2012) 1820.

[9] V. Vohra, K. Higashimine, T. Murakami, H. Murata, Appl. Phys. Lett. 101 (2012) 173301.

[10] V. Vohra, M. Campoy-Quiles, M. Garriga, H. Murata, J. Mater. Chem. 22 (2012) 20017.

[11] A. Orimo, K. Masuda, S. Honda, H. Benten, S. Ito, H. Ohkita, H. Tsuji, Appl. Phys. Lett. 96 (2010) 043305.

[12] D. Chen, A. Nakahara, D. Wei, D. Nordlund, T. P. Russell, Nano Lett. 11 (2011) 561.

[13] W. C. Tsoi, S. J. Spencer, L. Yang, A. M. Ballantyne, P. G. Nicholson, A. Turnbull, A. G. Shard, C. E. Murphy, D. D. C. Bradley, J. Nelson, J.-S. Kim, Macromolecules 44 (2011) 2944.